Provided for non-commercial research and education use.
Not for reproduction, distribution or commercial use.

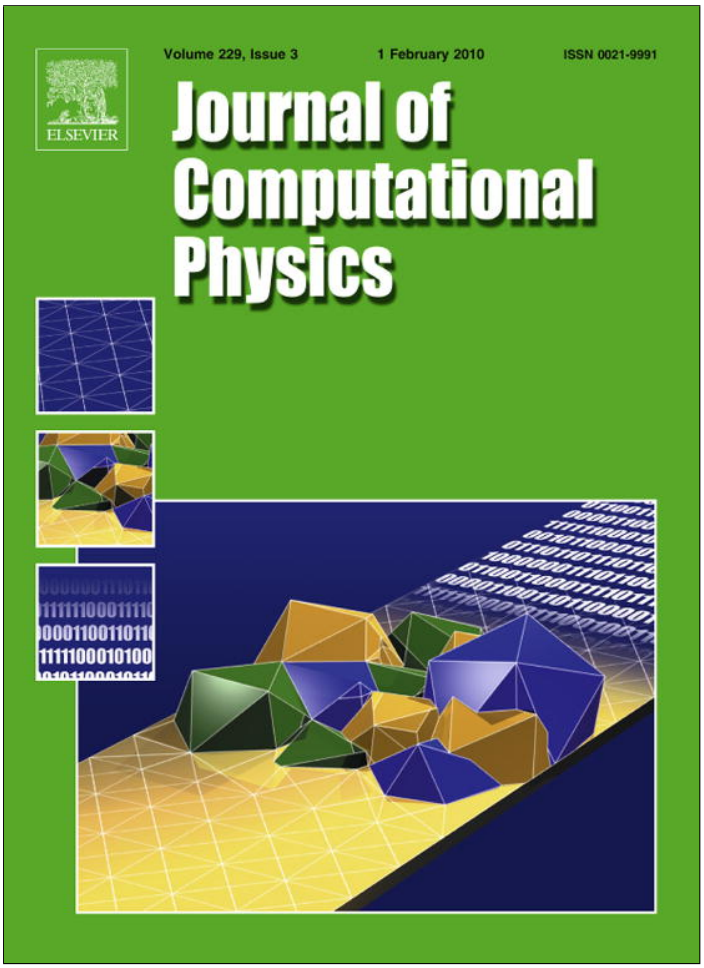

This article appeared in a journal published by Elsevier. The attached copy is furnished to the author for internal non-commercial research and education use, including for instruction at the authors institution and sharing with colleagues.

Other uses, including reproduction and distribution, or selling or licensing copies, or posting to personal, institutional or third party websites are prohibited.

In most cases authors are permitted to post their version of the article (e.g. in Word or Tex form) to their personal website or institutional repository. Authors requiring further information regarding Elsevier's archiving and manuscript policies are encouraged to visit:

http://www.elsevier.com/copyright

Author's personal copy

Journal of Computational Physics 229 (2010) 728–744

Contents lists available at ScienceDirect

Journal of Computational Physics

journal homepage: www.elsevier.com/locate/jcp

Modeling electrokinetic flows in microchannels using coupled lattice Boltzmann methods

Moran Wang *, Qinjun Kang

Los Alamos National Laboratory, Mail Stop T003, Los Alamos, NM 87545, United States

ARTICLE INFO

Article history:
Received 24 October 2008
Received in revised form 24 September 2009
Accepted 3 October 2009
Available online 12 October 2009

Keywords:
Electrokinetic flows
Lattice Boltzmann method
Multiphysical transport
Poisson–Boltzmann model
Dynamic model
Microfluidics and nanofluidics

ABSTRACT

We present a numerical framework to solve the dynamic model for electrokinetic flows in microchannels using coupled lattice Boltzmann methods. The governing equation for each transport process is solved by a lattice Boltzmann model and the entire process is simulated through an iteration procedure. After validation, the present method is used to study the applicability of the Poisson–Boltzmann model for electrokinetic flows in microchannels. Our results show that for homogeneously charged long channels, the Poisson–Boltzmann model is applicable for a wide range of electric double layer thickness. For the electric potential distribution, the Poisson–Boltzmann model can provide good predictions until the electric double layers fully overlap, meaning that the thickness of the double layer equals the channel width. For the electroosmotic velocity, the Poisson–Boltzmann model is valid even when the thickness of the double layer is 10 times of the channel width. For heterogeneously charged microchannels, a higher zeta potential and an enhanced velocity field may cause the Poisson–Boltzmann model to fail to provide accurate predictions. The ionic diffusion coefficients have little effect on the steady flows for either homogeneously or heterogeneously charged channels. However the ionic valence of solvent has remarkable influences on both the electric potential distribution and the flow velocity even in homogeneously charged microchannels. Both theoretical analyses and numerical results indicate that the valence and the concentration of the counter-ions dominate the Debye length, the electrical potential distribution, and the ions transport. The present results may improve the understanding of the electrokinetic transport characteristics in microchannels.

Published by Elsevier Inc.

1. Introduction

Multiphysical transport has attracted a lot of attention in recent years due to its increasingly important applications in biomedical, environmental, and energy engineering [1–5]. Electrokinetic flow, which involves multiple processes including fluid flow, electrostatic interaction, species diffusion, and sometimes energy transfer, is one of the most typical multiphysical transport phenomena because of the ubiquitousness of the electrolyte solution in nature and engineering applications [6,7]. Although numerous theories and models for large-scale electrokinetic flows have been developed for almost one century [6,8], only in recent decades has the electrokinetic transport shown awakening importance for various applications, especially at micro- and nanoscale. For instance, a better understanding of nanoscale electrokinetic flows will help understand the mass and information transport in ion channels in cells [9,10]. Accurate predictions of electroosmotic flow in microfluidic devices may shed light on optimal designs of bio-macromolecules diagnostics [2,11–13] and microscale energy systems like

* Corresponding author. Tel.: +1 505 6640698; fax: +1 505 6658737.
E-mail addresses: mwang@lanl.gov (M. Wang), qkang@lanl.gov (Q. Kang).

0021-9991/$ - see front matter Published by Elsevier Inc.
doi:10.1016/j.jcp.2009.10.006

Author's personal copy

micro fuel cells [5] and batteries [14,15]. Electrokinetic flow is also an important non-mechanical actuating technique for microfluidics [12], and has been widely applied for pumping [16–18], mixing [19–21], and separating [11].

The Poisson–Boltzmann (PB) model, which is composed of a Navier–Stokes equation for fluid flow and a PB equation for electric potential distribution, has been widely used for analysis and prediction of electrokinetic flows in microchannels [6,22]. The Boltzmann distribution assumption of ions in electric double layer (EDL) leads to the decoupling between the fluid flow and the ion distribution, which makes the predictions much easier. Many algorithms and analyses based on the PB model have been proposed for the understanding of electrokinetic fluid mechanics and optimization of electrokinetic microdevices [23–28]. However the Boltzmann distribution is an equilibrium model and its applicability is restricted by its preconditions. The applicability of the Boltzmann distribution is questionable when ions have macroscopic motion (advection or diffusion), surface is heterogeneously charged, or the bulk solution boundary condition is not satisfied in the place sufficiently far away from the charged surface [6]. A more general model is the dynamic model which utilizes the Nernst–Planck equation for ions transport instead of the hypothesized Boltzmann distribution [29]. In the dynamic model, each transport process is governed by the corresponding fundamental dynamic equation. The dynamic model has been used to validate the PB model by a few researchers [30–34], and it was reported that the PB model failed in the cases of overlapped double layers [31,33]. However a careful review of the previous work reveals inconsistencies in the boundary treatment between different models, which may be responsible for the discrepancy between the dynamic and PB model predictions. Therefore the applicability of the PB model needs to be revisited more carefully.

Because the transport processes are influenced by each other, the governing equations in the dynamic model are coupled together, which poses a great challenge to the numerical solution. There are several efforts in the literature to numerically solve the coupled governing equations in the dynamic model based on the traditional PDE solvers, such as the finite-difference method (FDM) [30,32], the finite volume method (FVM) [35,36] and the finite element method (FEM) [37]. Recently Lu et al. [38] presented a hybrid framework combining finite element and boundary element methods to solve the Poisson–Nernst–Planck (PNP) equation for electrodiffusion. Hlushkou et al. [39] proposed a coupled lattice Boltzmann and finite-difference method to solve the dynamic model for electroosmosis in microchannels, in which the lattice Boltzmann method (LBM) was used to model fluid flow and other governing equations were solved by the FDM. This is a good attempt to take advantage of the flexibility and efficiency of the LBM. However the boundary condition might be inconsistent between these two methods on the same set of grid [40]. He and Li [41] proposed a multiple LBM procedure for the electrochemical systems, but they used a local neutrality law to constrain the electric potential distribution which could be inaccurate for charged colloids [42].

The objectives of this contribution are to: (1) present a coupled LB algorithm and framework to solve the governing equations in the dynamic model for the multiphysical transport in electrokinetic flows in microchannels; (2) clarify the ambiguities in the literature on the applicability of the PB model by simulating the electroosmotic flows in microchannels using the dynamic model and comparing the results with those from the PB model. The paper is organized as follows. In Section 2 we introduce the governing equations and the boundary conditions of the dynamic model. In Section 3, we present our evolution equations for all the transport processes and the coupling framework. In Section 4, after validating the accuracy and efficiency of the code, we investigate the applicability of the PB model in homogeneously and heterogeneously charged microchannels by comparing the results from the dynamic model and the PB model. In addition, some studies that have never been done using the PB model will also be carried out and the results will be presented.

2. Mathematical models

2.1. Governing equations

Since our scale of interest is much larger than the atomistic scale, the macroscopic hydrodynamic and electrodynamic equations are still valid. For a multi-component constant-property Newtonian electrolyte fluid flowing in a microchannel with no mass source, the governing equations for laminar flow are [6,43,44]

$$\frac{\partial \rho}{\partial t} + \nabla \cdot (\rho \mathbf{u}) = 0, \tag{1}$$

and

$$\frac{\partial (\rho \mathbf{u})}{\partial t} + \mathbf{u} \cdot \nabla (\rho \mathbf{u}) = -\nabla p + \nabla \cdot [\nu \nabla (\rho \mathbf{u})] + \mathbf{F}, \tag{2}$$

where ρ represents the density of the fluid, t the time, $\mathbf{u}$ the velocity vector, p the pressure, ν the kinetic viscosity, and $\mathbf{F}$ the body force density which may include all the effective body forces such as the electrical field force. In the case of incompressible flows, the pressure gradient can be conveniently included in $\mathbf{F}$ [26,45]. In this work, the fluid is only driven by the electrical field force and the pressure gradient is zero in the entire computational domain.

For the ith ion species in the solute, the mass conservation equation describing transport and reaction can be written in the general form [46]:

$$\frac{\partial C_i}{\partial t} + \nabla \cdot \mathbf{J}_i + \lambda_i C_i = R_i, \tag{3}$$

Author's personal copy

where C_i denotes the ionic concentration, $\mathbf{J}_i$ the species flux, λ_i a radioactive decay constant, and R_i the rate at which the ith species is produced or consumed by chemical reactions. The flux $\mathbf{J}_i$, in general, consists of contributions from advection, diffusion and dispersion in addition to an electrochemical migration term. Neglecting dispersion, the flux has the form [46]

$$\mathbf{J}_i = -\frac{ez_iD_i}{kT}C_i\nabla\Psi - D_i(\nabla C_i + C_i\nabla\ln\gamma_i) + C_i\mathbf{u}, \tag{4}$$

where the first term on the right refers to electrochemical migration, the second term to aqueous diffusion, and the last term to advective transport. This is the famous Nernst–Planck equation [29]. Here z_i, D_i and γ_i denote the ion algebraic valence, the diffusivity and the activity coefficient of the ith species, respectively; and e, k, and T denote the absolute charge of electron, the Boltzmann constant and the absolute temperature, respectively. The quantity Ψ represents the local electrical potential caused by the ionic distribution which is governed by the Poisson equation [6]

$$\nabla\cdot(\varepsilon_r\varepsilon_0\nabla\Psi) = -\rho_e = -\sum_i ez_iC_i, \tag{5}$$

where ε_r is the local dimensionless fluid dielectric constant, ε_0 the permittivity of a vacuum, and ρ_e the net charge density.

Eqs. (1)–(5) govern the hydrodynamic and electrodynamic transport processes in electrokinetic flows. For isothermal incompressible uniform fluids with no polarization, radiation or chemical reactions, these equations can be further simplified as

$$\nabla\cdot\mathbf{u} = 0, \tag{6}$$

$$\frac{\partial\mathbf{u}}{\partial t} + \mathbf{u}\cdot\nabla\mathbf{u} = \nu\nabla^2\mathbf{u} + \frac{\mathbf{F}}{\rho}, \tag{7}$$

$$\frac{\partial C_i}{\partial t} + \mathbf{u}\cdot\nabla C_i = D_i\nabla^2C_i + \frac{ez_iD_i}{kT}\nabla\cdot(C_i\nabla\Psi), \tag{8}$$

and

$$\nabla^2\Psi = -\frac{\rho_e}{\varepsilon_r\varepsilon_0}, \tag{9}$$

where $\mathbf{F}$ can be any kind of effective body force. In this contribution we only consider the static electrical force from an external electric field. The general form of electrical force in microscale electrokinetic fluids can be expressed as [26]:

$$\mathbf{F}_E = -\rho_e\nabla\Psi_{ext}, \tag{10}$$

where Ψ_{ext} is the external electrical potential field. Since the velocity of the electrokinetic flows in microchannels is very low, the electromagnetic susceptibility is negligible.

When the ionic convection is negligible and the electric potential is continuously derivable, Eq. (8) has a simple steady solution for dilute electrolyte solutions:

$$C_i = C_{i,\infty}e^{-\frac{ez_i\Psi}{kT}}. \tag{11}$$

Substituting Eq. (11) into Eq. (9) yields the famous nonlinear PB equation [47]:

$$\nabla^2\Psi = -\frac{1}{\varepsilon_r\varepsilon_0}\sum_i ez_iC_{i,\infty}\exp\left(-\frac{ez_i}{kT}\Psi\right). \tag{12}$$

The PB model leads to the decoupling of the electric potential distribution from the fluid flow, which makes the solution much easier than the dynamic model. The PB model has been numerically solved by numerous methods successfully [18,23,24,26,27,32,40,48–50].

2.2. Boundary conditions

We assume a longitudinal spatial periodicity for the finite domain under consideration because the length of a microfluidic channel is usually very large compared to the width. The periodic boundary conditions include the continuities between inlet and outlet:

$$C_{i,inlet} = C_{i,outlet}, \tag{13}$$

$$\mathbf{u}_{inlet} = \mathbf{u}_{outlet}, \tag{14}$$

and the constant gradient of the external electrical field:

$$\mathbf{E} = -\nabla\Psi_{ext}. \tag{15}$$

At the liquid–solid interface Ω, the non-slip velocity and the zero normal flux conditions are applied:

$$\mathbf{u}_\Omega = 0 \quad , \tag{16}$$

Author's personal copy

$$(\mathbf{v}\cdot\mathbf{J}_i)_\Omega = 0, \tag{17}$$

where $\mathbf{v}$ is the outer unit vector normal to Ω. In case of chemical reactions occurring at the interface, the normal flux is related to the reaction rates. Substituting Eq. (4) into Eq. (17) leads to:

$$\frac{(\mathbf{v}\cdot\nabla C_i)_\Omega}{C_i} = -\frac{ez_i}{kT}(\mathbf{v}\cdot\nabla\Psi)_\Omega. \tag{18}$$

Integrate both sides of Eq. (18) on the boundary and we can further simplify the boundary condition as:

$$C_{i,\Omega} = C_{i,m}e^{-\frac{ez_i}{kT}(\zeta-\Psi_m)}, \tag{19}$$

where $C_{i,m}$ and Ψ_m denote the ith ionic concentration and the electrical potential at the middle of the channel respectively, and ζ is the zeta potential. Thus the boundary condition for ionic concentration becomes a simple Dirichlet-type one. The simplification of Eq. (19) can improve the computational efficiency significantly and therefore has been frequently employed in previous work [30,32,35,36].

The electrical potential at the interface can be imposed through either the surface charge density (σ) or the zeta potential (ζ). The former leads to the Neumann-type and the latter to the Dirichlet-type boundary conditions, respectively. A recent study using the LBM has proved that these two types of boundary conditions are consistent, but the latter one has a better computational efficiency [49]. Therefore we use the Dirichlet boundary condition for the electric potential equation (Eq. (9)):

$$\psi_\Omega = \zeta. \tag{20}$$

3. Numerical methods

The governing equations are solved using coupled multiple LBMs. The LBM is a relatively new numerical method for simulating complex flow and transport phenomena [51,52]. Unlike conventional computational methods based on macroscopic continuum equations, in the LBM, the mesoscopic Boltzmann equation is used to determine macroscopic transport dynamics, and the governing equations are solved by tracking distribution functions of species packets on lattices [53]. The LBM is flexible, broadly applicable, and straightforwardly adaptable for parallel computing. Due to the ease of incorporating complex boundary conditions, it has been successfully applied to multiphase and multi-component transport [54,55], multi-physicochemical transport through porous media [50,56,57], and solid particle suspensions [58–61].

In the rest of this section we introduce the LB evolution equations, the boundary treatments, and the flow scheme of our numerical framework.

3.1. Evolution equations

3.1.1. Evolution equation for hydrodynamics

The evolution equation for laminar flow driven by an external force has the form [51,62]

$$f_\alpha(\mathbf{r}+\mathbf{e}_\alpha\delta_t, t+\delta_t) - f_\alpha(\mathbf{r},t) = -\frac{1}{\tau_v}\left[f_\alpha(\mathbf{r},t) - f_\alpha^{eq}(\mathbf{r},t)\right] + \delta_t F_\alpha, \tag{21}$$

where $\mathbf{r}$ denotes the position vector, $\mathbf{e}_\alpha$ the discrete velocities, δ_t the time step, and τ_v the dimensionless relaxation time.

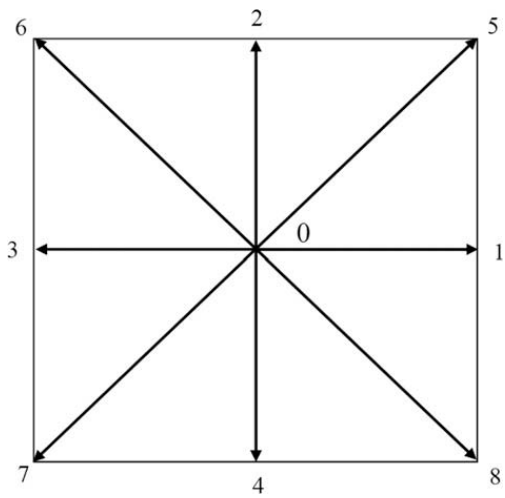

Fig. 1. Direction system for D2Q9 model.

Author's personal copy

For the commonly used two-dimensional nice-speed (D2Q9) model shown in Fig. 1, the discrete velocities are,

$$\mathbf{e}_\alpha = \begin{cases} (0,0) & & \alpha = 0 \\ (\cos\theta_\alpha, \sin\theta_\alpha)c, & \theta_\alpha = (\alpha-1)\pi/2 & \alpha = 1-4 \\ \sqrt{2}(\cos\theta_\alpha, \sin\theta_\alpha)c, & \theta_\alpha = (\alpha-5)\pi/2 + \pi/4 & \alpha = 5-8 \end{cases}, \tag{22}$$

where c is the lattice speed defined as δ_x/δ_t, δ_x the lattice constant (grid size). The density equilibrium distribution f_α^{eq} can thus be expressed as [51,63]

$$f_\alpha^{eq} = \omega_\alpha \rho \left[1 + 3\frac{\mathbf{e}_\alpha \cdot \mathbf{u}}{c^2} + 9\frac{(\mathbf{e}_\alpha \cdot \mathbf{u})^2}{2c^4} - \frac{3\mathbf{u}^2}{2c^2} \right], \tag{23}$$

with

$$\omega_\alpha = \begin{cases} 4/9 & \alpha = 0 \\ 1/9 & \alpha = 1-4 \\ 1/36 & \alpha = 5-8 \end{cases} \tag{24}$$

The relaxation time for fluid flow is related with the fluid viscosity by

$$\tau_\nu = \frac{3\nu}{c\delta_x} + 0.5, \tag{25}$$

For the electrokinetic flow in a long microchannel driven by an external electric field, the external force in the discrete LB equation is [64]

$$F_\alpha = \frac{3\rho_e \mathbf{E} \cdot (\mathbf{e}_\alpha - \mathbf{u})}{\rho c^2} f_\alpha^{eq}. \tag{26}$$

After evolution, the macroscopic density and velocity can be calculated using

$$\rho = \sum_\alpha f_\alpha, \tag{27}$$

$$\rho\mathbf{u} = \sum_\alpha \mathbf{e}_\alpha f_\alpha. \tag{28}$$

3.1.2. Evolution equations for ion transport

Inspired by the process of LBM solving the Navier–Stokes equation, people have proposed several models for solving the advection-diffusion equations [26,64–66]. We use the following evolution equation to solve the ion transport governing equation for the ith ion species, Eq. (8) [26,49,66]:

$$g_\alpha(\mathbf{r} + \mathbf{e}_\alpha \delta_{t,D_i}, t + \delta_{t,D_i}) - g_\alpha(\mathbf{r}, t) = -\frac{1}{\tau_{D_i}}\left[g_\alpha(\mathbf{r}, t) - g_\alpha^{eq}(\mathbf{r}, \mathbf{t})\right] + \omega_\alpha \delta_{t,D_i}\left(1 - \frac{0.5}{\tau_{D_i}}\right)\frac{ez_i D_i}{kT}\nabla \cdot (C_i \nabla \Psi), \tag{29}$$

where τ_{D_i} is the dimensionless relaxation time for the ith ion transport related to the diffusion coefficient D_i, and δ_{t,D_i} the corresponding time step.

For a D2Q9 lattice system, the equilibrium distribution is [64,66]

$$g_\alpha^{eq} = \begin{cases} -\frac{2C_i}{3}\frac{\mathbf{u}^2}{c_{D_i}^2} & \alpha = 0 \\ \frac{C_i}{9}\left[\frac{3}{2} + \frac{3}{2}\frac{\mathbf{e}_\alpha \cdot \mathbf{u}}{c_{D_i}^2} + \frac{9}{2}\frac{\mathbf{e}_\alpha \cdot \mathbf{u}}{c_{D_i}^2} - \frac{3}{2}\frac{\mathbf{u}^2}{c_{D_i}^2}\right] & \alpha = 1-4 \\ \frac{C_i}{36}\left[3 + 6\frac{\mathbf{e}_\alpha \cdot \mathbf{u}}{c_{D_i}^2} + \frac{9}{2}\frac{\mathbf{e}_\alpha \cdot \mathbf{u}}{c_{D_i}^2} - \frac{3}{2}\frac{\mathbf{u}^2}{c_{D_i}^2}\right] & \alpha = 5-8 \end{cases} \tag{30}$$

and the dimensionless relaxation time is calculated by [49]

$$\tau_{D_i} = \frac{3D_i}{2c_{D_i}\delta_x} + 0.5, \tag{31}$$

with c_{D_i} representing the diffusion lattice speed for the ith ion. The value of c_{D_i} is independent of c in Eq. (25) and can be assigned any positive value as long as the value of τ_{D_i} is within (0.5,2) [49,66]. Different values of c_{D_i} lead to different time steps for each ion transport evolution since

$$\delta_{t,D_i} = \delta_x / c_{D_i}. \tag{32}$$

The final ionic concentration for the ith ion can be calculated after evolution by

Author's personal copy

$$C_i = \sum_\alpha g_\alpha + \frac{\delta_{t,D_i}}{2}\frac{ez_iD_i}{kT}\nabla\cdot(C_i\nabla\Psi). \tag{33}$$

3.1.3. Evolution equation for electrodynamics

In order to solve the static electrodynamics equation, Eq. (9), using LBM, we rewrite it by adding a time-dependent term [49]:

$$\frac{\partial\Psi}{\partial t} = \nabla^2\Psi + \frac{\rho_e}{\varepsilon_r\varepsilon_0}. \tag{34}$$

The evolution equation for the electrical potential on the two-dimensional discrete lattices can then be written as [26,49,66]

$$h_\alpha(\mathbf{r}+\Delta\mathbf{r}, t+\delta_{t,\psi}) - h_\alpha(\mathbf{r},t) = -\frac{1}{\tau_\psi}\left[h_\alpha(\mathbf{r},t) - h_\alpha^{eq}(\mathbf{r},t)\right] + \omega_\alpha\delta_{t,\psi}\left(1-\frac{0.5}{\tau_\psi}\right)\frac{\rho_e}{\varepsilon_r\varepsilon_0}, \tag{35}$$

where τ_ψ is the dimensionless relaxation time for electrical potential transport and $\delta_{t,\psi}$ the time step.

Again for a D2Q9 lattice system, the equilibrium distribution of the electric potential evolution function h is [26,49]

$$h_\alpha^{eq} = \begin{cases} 0 & \alpha = 0 \\ \frac{\Psi}{6} & \alpha = 1-4 \\ \frac{\Psi}{12} & \alpha = 5-8 \end{cases}. \tag{36}$$

The dimensionless relaxation time is calculated by [49]

$$\tau_\psi = \frac{3}{2c_\psi\delta_x} + 0.5, \tag{37}$$

where c_ψ is the electrostatic lattice speed, which, similar as c_{D_i}, can be any positive value only ensuring the relaxation time τ_ψ within (0.5, 2) [49]. The time step is given by

$$\delta_{t,\psi} = \frac{\delta_x}{c_\psi}. \tag{38}$$

The steady solution of the evolution Eq. (35) has been proved consistent with the macroscopic Poisson equation, Eq. (9). The macroscopic electrical potential can be calculated using [49]

$$\Psi = \sum_\alpha\left(h_\alpha + 0.5\delta_{t,\psi}\omega_\alpha\frac{\rho_e}{\varepsilon_r\varepsilon_0}\right). \tag{39}$$

3.2. Boundary condition implementations

Boundary treatments are very critical to any numerical methods. Since we are solving several governing equations on the same set of lattices, i.e., δ_x for all evolution equations is the same, the consistency of the boundary implementations is essential. Although the "bounce-back" model is popular and easy to use, it has only first-order accuracy. In this contribution, we introduce second-order accurate boundary conditions for all the models.

3.2.1. Non-slip model for hydrodynamics

For stationery walls, the unknown density distribution functions at the wall are determined from the local equilibrium distribution function with a "counter slip" velocity [67,68]. Take the upper wall as an example. The populations f_1, f_2, f_3, f_5 and f_6 are known from the previous evolution step, but f_4, f_7, and f_8 need to be determined from the boundary condition. The "counter slip" velocity is defined by

$$u' = 6\frac{-(f_1 - f_3 + f_5 - f_6)}{\rho'}c, \tag{40}$$

where

$$\rho' = 6(f_2 + f_5 + f_6). \tag{41}$$

Thus the unknown density distributions are calculated from the equilibrium distribution function

Author's personal copy

$$f_4 = \frac{1}{9}\rho'\left[1 + 3\frac{u'}{c} + 9\frac{(u')^2}{2c^2} - \frac{3(u')^2}{2c^2}\right], \tag{42a}$$

$$f_7 = \frac{1}{36}\rho'\left[1 + 3\frac{u'}{c} + 9\frac{(u')^2}{2c^2} - \frac{3(u')^2}{2c^2}\right], \tag{42b}$$

$$f_8 = \frac{1}{36}\rho'\left[1 + 3\frac{u'}{c} + 9\frac{(u')^2}{2c^2} - \frac{3(u')^2}{2c^2}\right]. \tag{42c}$$

3.2.2. Boundary treatment for ions

Several boundary treatment methods have been proposed to deal with the Dirichlet-type boundary conditions for advection-diffusion equations. Here we follow D'Orazio's approach [69,70] which is of second-order accuracy and consistent with the non-slip model for fluid flow. In this approach, the unknown populations are assumed to be from an equilibrium distribution at a concentration $C_{i,0}$ which is determined by the given constraints. Again for the upper wall, the unknown g_4, g_7, and g_8 can be obtained from the equilibrium distribution of $C_{i,0}$ which is:

$$C_{i,0} = 3C_{i,\Omega} - 3S_g - 1.5\delta_{t,D_i}\sum_{\alpha}\omega_\alpha \frac{ez_iD_i}{kT}\nabla\cdot(C_i\nabla\Psi), \tag{43}$$

where S_g is the sum of known populations coming from the internal nodes and nearest wall nodes

$$S_g = g_0 + g_1 + g_2 + g_3 + g_5 + g_6, \tag{44}$$

Thus the unknown distributions are

$$g_4 = C_{i,0}/6, \tag{45a}$$
$$g_7 = C_{i,0}/12, \tag{45b}$$
$$g_8 = C_{i,0}/12. \tag{45c}$$

3.2.3. Boundary treatment for electric potential

The Dirichlet boundary of electric potential can be treated similarly as that for ions [69,70]. Still for the upper wall, the h_4, h_7, and h_8 can be obtained from the equilibrium distribution of Ψ_0:

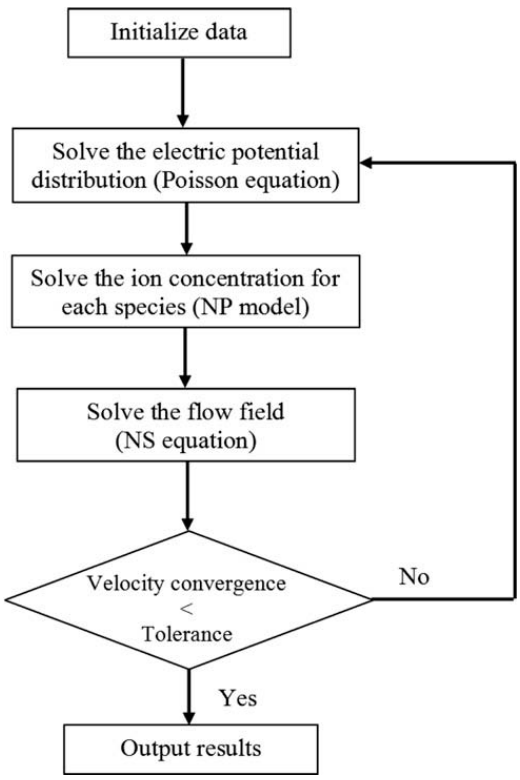

Fig. 2. Flow chart of the coupled lattice Boltzmann method.

Author's personal copy

$$\Psi_0 = 3\Psi_\Omega - 3S_h - 1.5\delta_{t,\psi}\sum_\alpha \omega_\alpha \frac{\rho_e}{\varepsilon_r\varepsilon_0}, \tag{46}$$

where S_h is the sum of known populations coming from the internal nodes and nearest wall nodes

$$S_h = h_0 + h_1 + h_2 + h_3 + h_5 + h_6, \tag{47}$$

Thus the unknown distributions are

$$h_4 = \Psi_0/6, \tag{48a}$$
$$h_7 = \Psi_0/12, \tag{48b}$$
$$h_8 = \Psi_0/12. \tag{48c}$$

3.3. Flow scheme of the numerical framework

Since the governing equations, Eqs. (6)–(10), are coupled together, we implement an iterative scheme as shown in Fig. 2. In each iteration procedure, the electric potential distribution is first obtained through the evolutions of electric potential to the steady state based on the evolution Eq. (35), in which the charge density is calculated from the ion distributions of the last iteration based on Eq. (5) (or from the initial state for the first iteration). Then, the ionic concentration for each species is calculated by the evolution Eq. (29) for N_{C_i} steps. The time step, δ_{t,D_i}, may differ for different ions, but the total time step within one iteration has to be the same value for all ions, i.e., $t_{total} = N_{C_i} \cdot \delta_{t,D_i}$. The last step in the iteration is to solve the evolution Eq. (21) to obtain the velocity field. The evolution number, $N_{\mathbf{v}}$, has to ensure the total time step in the iteration to be t_{total}, i.e., $N_{\mathbf{v}} = t_{total}/\delta_t$.

Thus the coupled governing equations are solved by the iterative multiple lattice evolution models. This scheme is able to simulate time-dependent process with a very low Reynolds number. In this contribution, we only apply it to steady flows.

To judge if the simulation reaches steady state or not, we define the total divergence rates for electric potential convergence and velocity convergence as

$$\delta_\Psi^{dr} = \sqrt{\sum_{\mathbf{r}} \left(\frac{\Psi^n(\mathbf{r}) - \Psi^{n-1}(\mathbf{r})}{\Psi^n(\mathbf{r})}\right)^2}, \tag{49}$$

$$\delta_{\mathbf{v}}^{dr} = \sqrt{\sum_{\mathbf{r}} \left(\frac{\mathbf{v}^n(\mathbf{r}) - \mathbf{v}^{n-1}(\mathbf{r})}{\mathbf{v}^n(\mathbf{r})}\right)^2}, \tag{50}$$

where $\mathbf{r}$ denotes the location vector, and the superscript "n" represents the nth iteration. The simulation stops and the results are assumed to be steady state once the divergence rate is less than a given error tolerance (typically 10^{-6}).

The current method preserves the advantages of the LBM and is suitable for complex flows and parallel computing [56,57]. Although only 2D problems are considered in this paper, the algorithm can be easily extended to 3D.

4. Results and discussion

In this section, we simulate the electrokinetic flows in homogeneously and heterogeneously charged microchannels using our coupled LB codes, and compare the results with the PB model, to validate our codes and to investigate the conditions under which the PB model will fail.

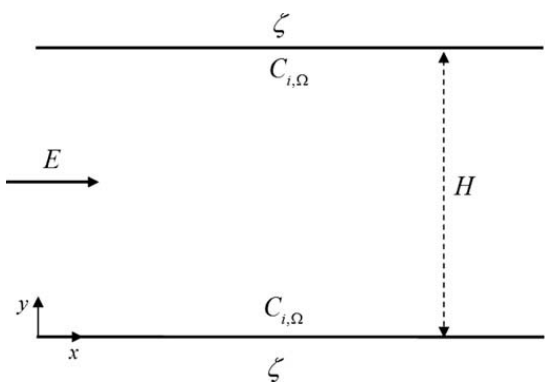

Fig. 3. The homogeneously charged microchannel.

Author's personal copy

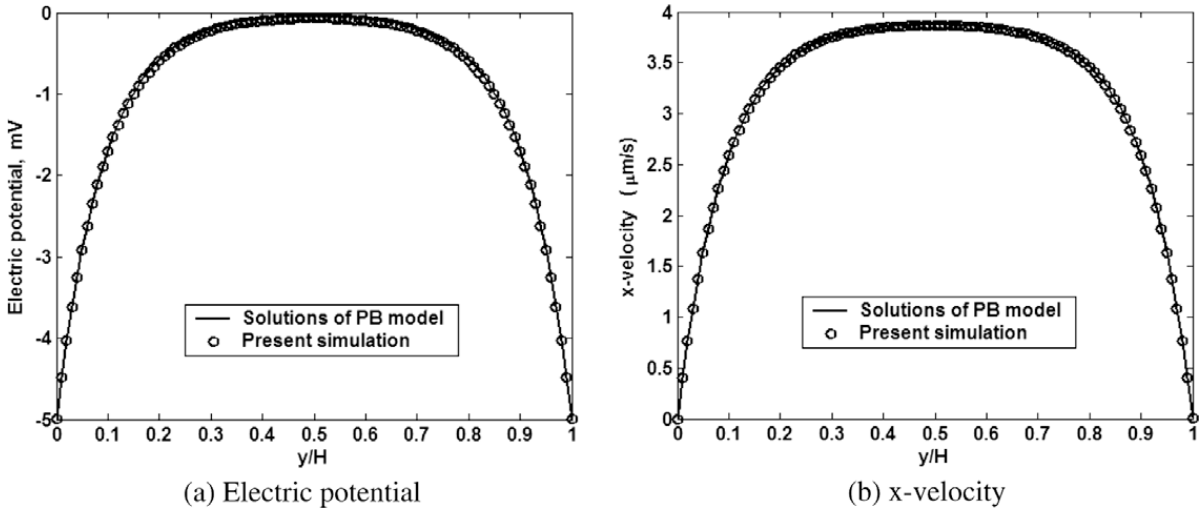

Fig. 4. Comparisons of electric potential and x-velocity distributions between the present simulation and the PB model.

4.1. Accuracy and efficiency

4.1.1. Benchmark

To validate the present algorithm and code, we first simulate the electroosmotic flow in a homogeneously charged microchannel, as shown in Fig. 3, with a width H of 1 μm. A 100×10 uniform grid is used. A 1:1 electrolyte solution is considered and the bulk ionic concentration $C_\infty = 10^{-5}$ M. The zeta potential for both walls is $\zeta = -5$ mV. The other properties and physical parameters are: the fluid density $\rho = 999.9\ \mathrm{kg/m^3}$, the dielectric constant $\varepsilon_r\varepsilon_0 = 6.95 \times 10^{-10}\ \mathrm{C^2/J\ m}$, the dynamic viscosity $\mu = 0.889$ m Pa s, the temperature $T = 273$ K, the diffusion coefficients for both ions $D_1 = D_2 = 1 \times 10^{-8}\ \mathrm{m^2/s}$ and $E = 1 \times 10^3$ V/m.

Since the x direction is periodic, there is no y-directional flow across the channel. Therefore the electric potential distribution obtained from the coupled dynamic equations, Eqs. (6)–(9), should be consistent with those from the PB model for thin EDL. Fig. 4 compares the electric potential and velocity profiles across the channel between the present simulations and the classical PB model. In the PB model, the electric potential is obtained by solving the nonlinear PB equations numerically and the velocity field is solved by the LPBM [26,45]. The ionic concentration is high enough for this case to ensure no interaction between the double layers of both walls. No chemical reactions are considered at the interfaces and the boundary conditions for the present dynamic equations are consistent with those for the PB model. The good agreement between the present dynamic model and the PB model validates the present algorithm and the codes.

4.1.2. Unphysical parameters

There are two unphysical parameters, the lattice speed (c) and evolution number per iteration (N). In the present algorithm they can influence the stability, the accuracy and the efficiency of simulations.

Since the physical characteristic times for fluid flow and species diffusions differ significantly, it is hard to find a common lattice speed to ensure that the dimensionless relaxation time (τ) for each evolution equation is within (0.5, 2). We use different lattice speeds for different evolution equations. Because all the boundary condition treatments employed are of second-order accuracy, the accuracy will not change with the value of the lattice speed [67]. As reported before, a larger lattice speed leads to a lower convergence speed [49], but a better stability. One has to balance between the stability and the convergence speed. For the present coupling algorithm, it is better to advance each iteration in a moderate level, i.e., not too drastic, to avoid numerical fluctuation or even divergence, especially for the ion transport.

The evolution number per iteration is the other unphysical parameter that needs to be optimized and balanced between accuracy and efficiency. To ensure the same total time step for each iteration, the evolution number has to satisfy

$$N_{C_1} \cdot \delta_{t,D_1} = N_{C_2} \cdot \delta_{t,D_2} = N_{\mathbf{v}} \cdot \delta_t, \tag{51}$$

where $N_{\mathbf{v}}$ is usually much greater than N_{C_1} and N_{C_2}.

Fig. 5 shows the maximum x-velocity for different evolution numbers per iterative step after finite iterative steps (500), and CPU time per iterative step, where $C_\infty = 10^{-5}$ M,$\zeta = -50$ mV,$E = 5 \times 10^6$ V/m and the other parameters are same as those in Section 4.1.1. The code was run on the Saguaro cluster at LANL, which has 64×2 AMD Opteron CPUs at 2.4 GHz. The results indicate that the simulated velocity becomes independent of N_{C_1} and stable when $N_{C_1} \geqslant 100$, but the CPU time increases sharply when $N_{C_1} \geqslant 2000$. Another calculation for 2:2 electrolyte solute shows that the simulated results becomes unstable again after $N_{C_1} \geqslant 2000$. Therefore for this case, N_{C_1} should be an integer within [100, 1000] for good accuracy and satisfactory efficiency. In all the following simulations of this work, we use $N_{C_1} = 1000$.

Author's personal copy

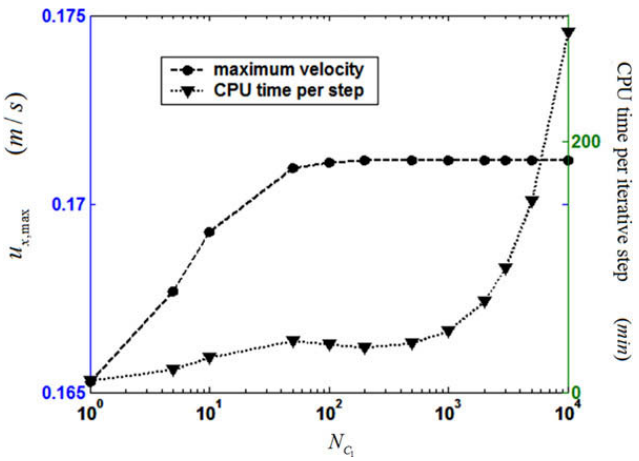

Fig. 5. Effects of evolution step number per iterative step on computational accuracy and efficiency.

4.2. Effects of the EDL thickness

The applicability of the PB model has been often questioned when the EDL is thick relatively to the channel width. Discrepancies have been reported between results of the PB model and the dynamic model and the breakdown of the PB model was always ascribed to the EDL overlap and interactions [30–32,35,36]. However, after a careful review of the previous work, we find that the inconsistent boundary conditions for different models may be the main reason for such deviations in these reports [31]. Our new algorithm and codes enable us to examine the effects of the EDL thickness on the applicability of the PB model.

Still for a long straight microchannel as shown in Fig. 3, we change the bulk ionic concentration C_∞ to vary the EDL thickness, namely the Debye length, defined as $\lambda = \sqrt{\varepsilon_0 \varepsilon_r kT/(2e^2 z_i^2 C_\infty)}$ for 1:1 electrolyte solution [6], and keep the other parameters the same as those in Section 4.1.1. Based on this definition, the EDL thickness for the case in Fig. 4 is 0.18 of the channel width, i.e., $\lambda = 0.18$ H.

Fig. 6 compares the results for different EDL thickness from the dynamic model and from the PB model. For the EDL thickness (λ) much smaller than the channel width (H), the ions distribution and flow velocities from both models are in excellent agreement, as shown in Fig. 4 and Fig. 6(a). When λ is comparable to H, like in Fig. 6(b), the ion distribution from the PB model begins to deviate from that from the dynamic model, though the deviation is very small ($< 1\%$). This deviation increases with the increase of the EDL thickness. However the velocity profiles from both models are still in good agreement even when λ is about 10 H as shown in Fig. 6(d). Unlike previous studies showing that the deviation appeared as soon as the EDLs overlapped, the present results show that the PB model is applicable for a wide range of EDL thickness. For ions distribution predictions, the PB model is accurate for λ no greater than H; while for flow modeling, the PB model is still applicable even for λ as large as 10 H.

4.3. Effects of heterogeneously charged surface

Heterogeneously charged surfaces are usually used to change the flow field or the wetting property of interfaces, which have many important applications in microfluidics, such as micromixing enhancement [19–21], bio-macromolecules separation, and microchip switch [13,71,72].

For the homogeneously charged long channel, there is no difference for the predicted electric potential distributions between the PB model and the dynamic (PNP and NS) model since the electric potential distribution is fully developed everywhere. However for the heterogeneously charged channel, the electric potential distribution is not developed, especially near the interface between surfaces charged differently, which may lead to deviation of the electric potential distribution predicted by the PB model from that by the dynamic model. Similar studies can be found in the "entry flow" [32] and in the step charged channels [30]. In this section, we are focusing on how the heterogeneous surface charge influences the electric potential distribution in the channel and whether these effects invalidate the PB model.

Fig. 7(a) shows a symmetrical arrangement of surface charge in a heterogeneously charged microchannel. Each wall is charged with uniform charge density, but with a boundary electric potential of ζ for one half and $-\zeta$ for the other half. The channel is also periodic in x direction. Fig. 7(b) shows a typical velocity vector field with four vertices in this domain.

4.3.1. Zeta potential effects

We first consider the effect of zeta potentials on the electric potential distribution. To avoid the effects from the velocity field, we set the external electric field strength to a low value: $E = 1 \times 10^3$ V/m. To exclude the effect from different diffusion coefficients, we set them to the same value for both ions: $D_1 = D_2 = 2 \times 10^{-9}$ m^2/s. The channel width is 1 μm and

Author's personal copy

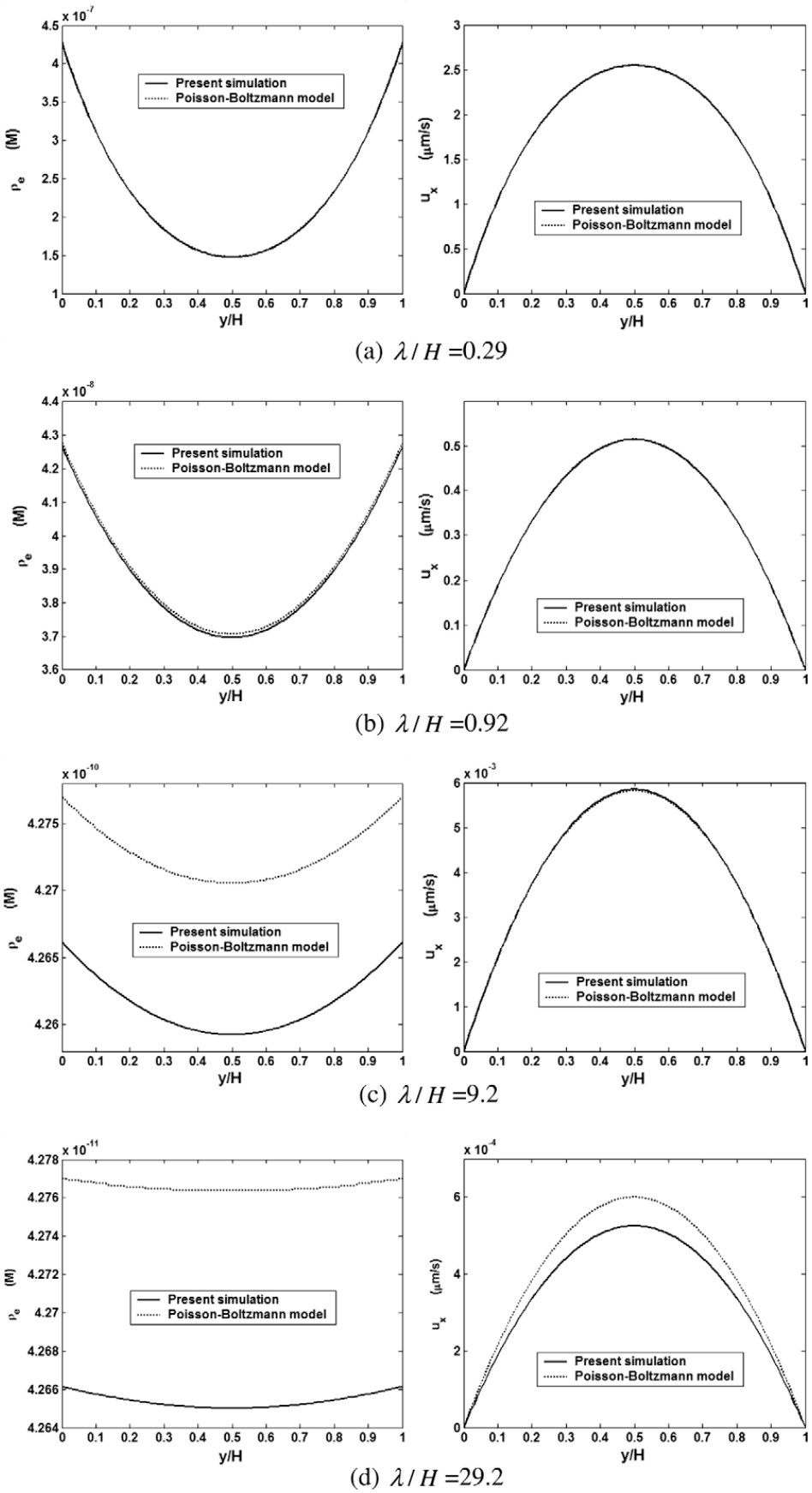

Fig. 6. Comparisons of net charge density and x-velocity profiles for different EDL thicknesses.

Author's personal copy

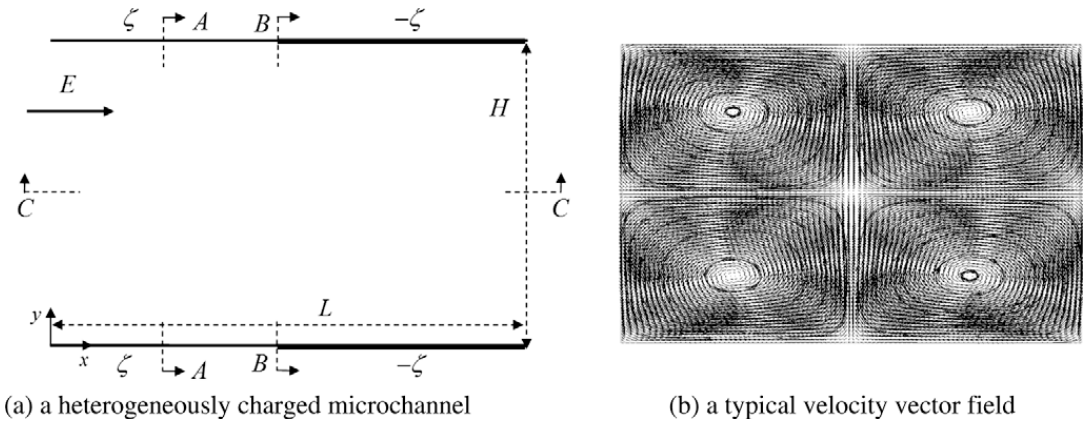

Fig. 7. Schematic of surface charge arrangement of a microchannel and its velocity field driven only by an external electric field.

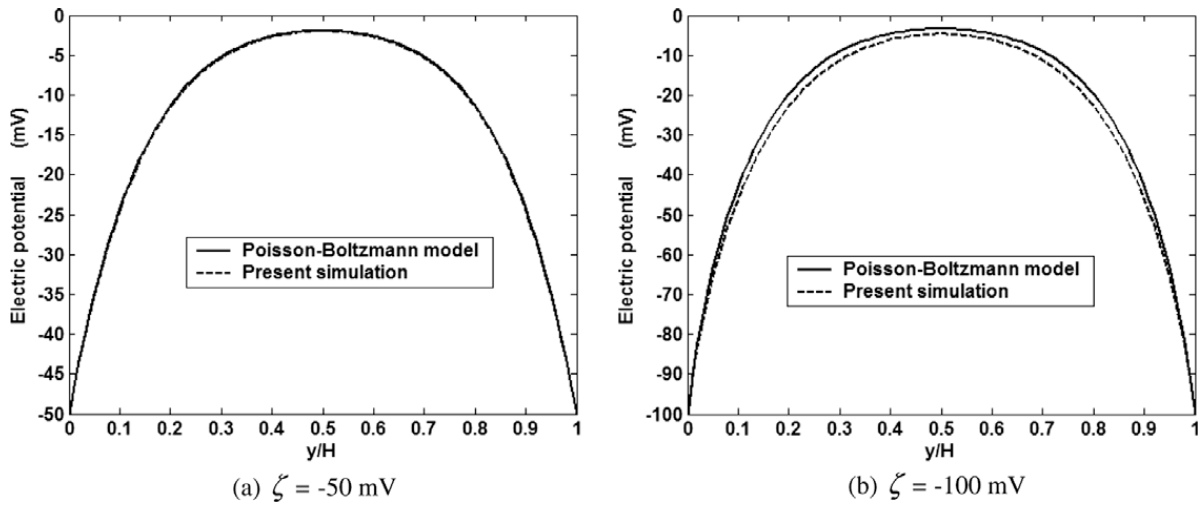

Fig. 8. Electric potential profiles at the A–A section for different zeta potentials.

100×100 grids are used. We vary the zeta potential ζ from -5 mV to -100 mV and keep the other parameters the same as those in Section 4.1.1.

When the absolute value of the zeta potential is small, such as 50 mV or lower, the electric potential distribution obtained from the PB model agrees well with that from the dynamic model. Fig. 8(a) shows the electric potential profiles at the A–A section when $\zeta = -50$ mV, where the two curves are almost the same. As the zeta potential increases, the result from the PB model begins to differ from that from the dynamic model. Fig. 8(b) illustrates the electric potential profiles for $\zeta = -100$ mV. For a high zeta potential, the electric potential profile predicted from the dynamic model is not as developed as that from the PB model. This result indicates that it is necessary to replace the PB model with the present dynamic (PNP and NS) model for heterogeneously charge surfaces with high zeta potentials.

4.3.2. Velocity field effects

Since the streamlines are not parallel to the surfaces any more for heterogeneously charged channels, the convection of ions will change the ions distribution and may consequently influence the electric potential distribution. Similar cases can be found even in homogeneously charged channels with blocks, where the velocity field is changed by the geometry. For heterogeneously charged channels, the advection strength can be easily controlled by varying the external electric field strength (E). Fig. 9 shows the electric potential distributions at the A–A and the C–C sections and corresponding x-velocity profiles for different ionic advection strength controlled by the electric field strength (E). The zeta potential is $\zeta = -50$ mV and the external electric field strength vary from 1×10^3 to 2×10^7 V/m. The other parameters are the same as those in 4.3.1.

When the electric field strength is small, such as $E = 1 \times 10^3$V/m, the ions advection is weak and negligible so that the electric potential distribution from the dynamic model almost coincides that from the PB model. As the driving force increases, the ions advection becomes stronger and the predicted electric potential distribution deviates more from the PB predictions. When $E = 1 \times 10^6$ V/m which can be actually easily realized in experiments, the maximum relative error between the two models for the electric potential is as large as 172%. This result indicates that the present dynamic model

Author's personal copy

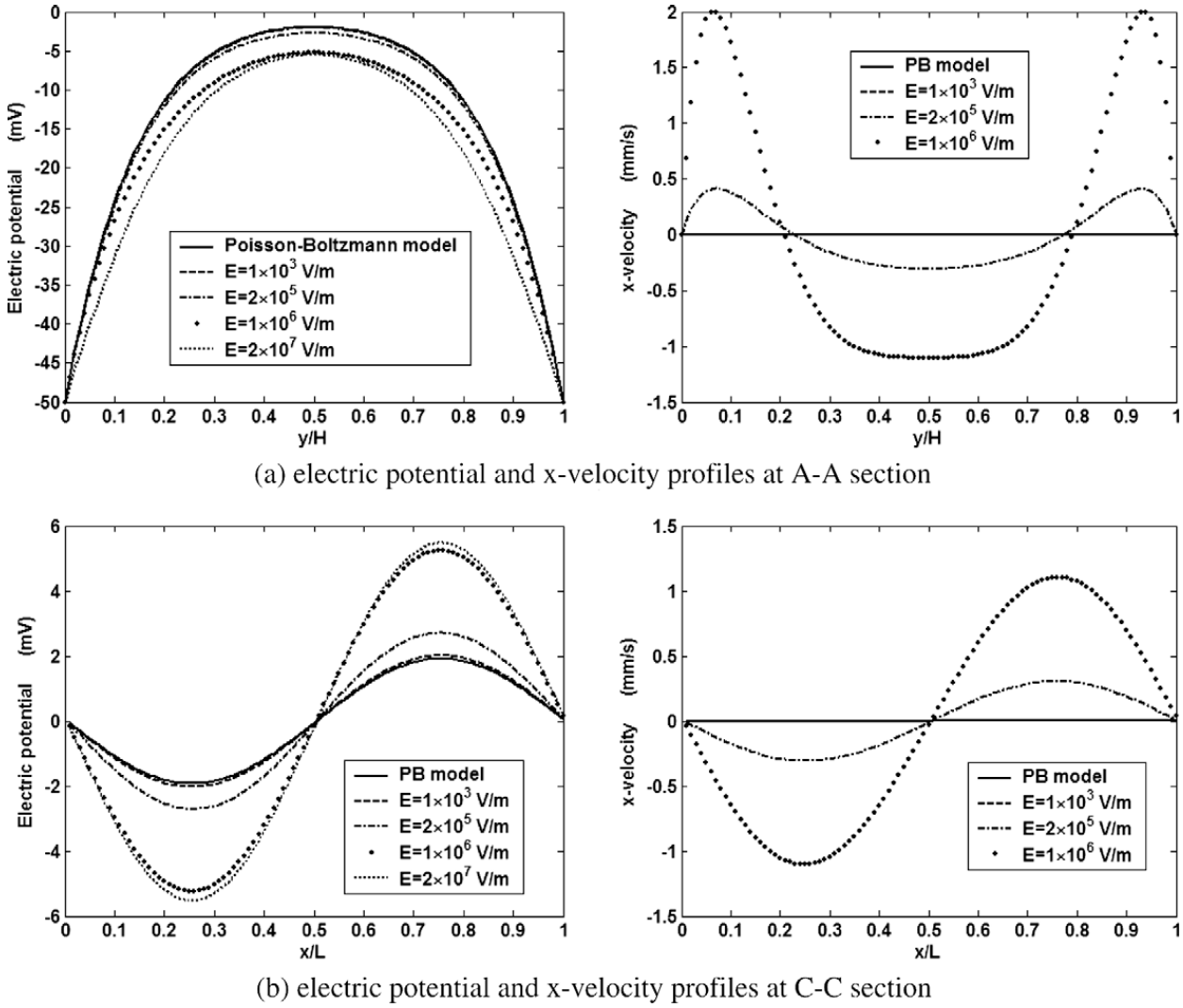

Fig. 9. Velocity field effects on the electric potential distributions controlled by the external electric field strength for heterogeneously charged microchannels.

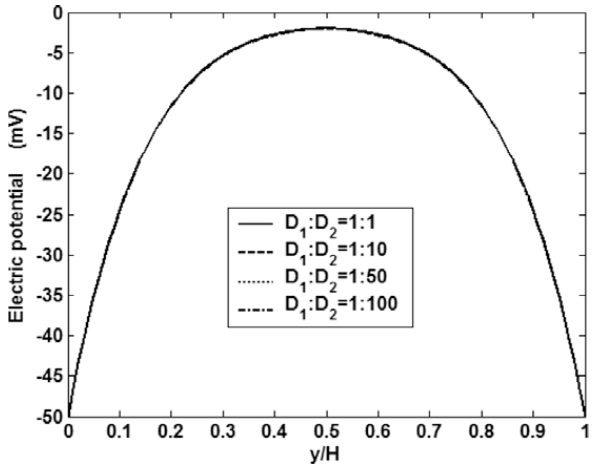

Fig. 10. Electric potential profiles for different ionic diffusion coefficient ratios at the A–A section.

will better predict and interpret results for the applications of heterogeneously charged channels, such as micromixing enhancements by electrokinetic flows.

Author's personal copy

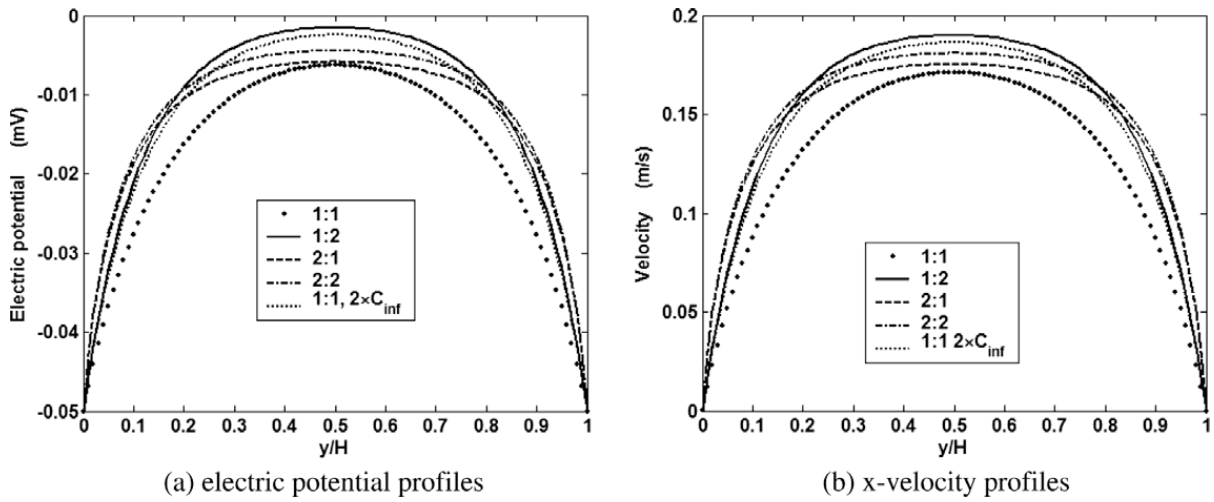

Fig. 11. Electric potential and velocity distributions in homogeneously charged channels for different ionic valence ratios.

Besides the external electric field strength, the velocity field can be also influenced by many other factors. For examples, the ionic advection in the heterogeneously charged channel is also related to the ionic concentration ($C_{i,\infty}$), the fluid viscosity ν, and the zeta potential (ζ). In engineering applications, the flow may also be driven by other forces, such as pressure gradient (Δp). The channel may not be a smooth straight one if there are blocks or roughness and cavitations inside. Each of these factors may lead to considerable contribution of ionic advection to the ion redistribution. For these cases, the present model will provide more accurate predictions.

4.3.3. Diffusion coefficient effect

Since the electric potential distribution in a heterogeneously charged microchannel is not fully developed, it is interesting to find out whether the ionic diffusion coefficients and their differences have any influence on the electric potential distributions. For the same microchannel as above, we change the diffusion coefficient values and their ratios from 1:1 to 1:100. Fig. 10 shows the electric potential profiles at the A–A section for different ionic diffusion coefficients, where $\zeta = -50$ mV,$E = 1 \times 10^3$ V/m and the other parameters are same as those in Section 4.3.1. The results indicate that the effect from the ionic diffusion coefficients is negligible for the electroosmotic flows in long microchannels. The reason may be that the characteristic time of ionic diffusion is much smaller than those of fluid flow and ions advection.

4.4. Effects of ionic valence

Although the multi-valence ions have been reported to influence nanoscale electrokinetic transport greatly [73,74], the effects of ionic valence on the electroosmotic flows in microchannels have never been investigated to the best of the authors' knowledge. The reason is that the net charge term (ρ_e) is hard to be linearized if the absolute value of valence ratio $|z_1 : z_2|$, is not 1:1. However it is not a problem for the present algorithm because there is no need for linearization at all.

Consider a homogeneously charged microchannel as shown in Fig. 3. The bulk solvent concentration $C_\infty = 1 \times 10^{-5}$ M, the external electric field strength $E = 5 \times 10^6$ V/m, the zeta potential $\zeta = -50$ mV and the other parameters are the same as those in Section 4.1.1. Fig. 11 compares the electric potential and velocity distributions for different ionic valence ratios. Four cases are considered: $|z_1 : z_2| = 1:1, 1:2, 2:1$ and 2:2, respectively. z_1 denotes the valence of the positive ions and z_2 that of the negative ones. For the 1:1 valence ratio, the results from a double bulk solvent concentration ($2C_\infty$) are also plotted in the same figures. The results show: (1) the ionic valence does influence the electric potential distribution and the velocity profile in electroosmotic flows. Among the different valence ratios, the 1:1 case leads to the smallest averaged electric potential (absolute value) and velocity across the channel when the other conditions are the same. The electric potential profiles and velocity distributions for the 2:1 and 2:2 valence ratios are close; while those results for the 1:2 valence at a bulk ionic concentration of C_∞ and the 1:1 valence ratio at 2 C_∞ are close. (2) The corresponding Debye length varies with the valence ratio as well. Fig. 11(a) indicates that the EDLs for 1:1 and 1:2 valence ratios are thicker than those for 2:1 and 2:2 ones. The valence number of positive ions seems to dominate the Debye length in the present negatively charged walls.

Our results apparently contradicts a popular definition of the Debye length [75]

$$\lambda = \sqrt{\varepsilon_0 \varepsilon_r kT / e \sum_i z_i^2 C_{i,\infty}}, \tag{52}$$

which will lead to the same Debye length between 1:2 and 2:1 valence ratios.

To understand these results, let us revisit the original PB equation, Eq. (12), for two-species/ions solutions:

Author's personal copy

$$\nabla^2 \Psi = -\frac{\rho_{e,\infty}}{\varepsilon_r \varepsilon_0}\left[\exp\left(-\frac{e}{kT} z_1 \Psi\right) - \exp\left(-\frac{e}{kT} z_2 \Psi\right)\right], \tag{53}$$

where $\rho_{e,\infty} = ez_1 C_{1,\infty} = -ez_2 C_{2,\infty}$ denotes the bulk charge density, z_1 is positive and z_2 negative, $C_{1,\infty}$ and $C_{2,\infty}$ are the species bulk ionic concentrations for positive and negative ions, respectively. For $|z_1 : z_2| = N : N, C_{1,\infty} = C_{2,\infty} = C_\infty$. When $|z_1 : z_2| = 1 : 2, C_{1,\infty} = 2\ C_\infty$ and $C_{2,\infty} = C_\infty$. If $|z_1 : z_2| = 2 : 1, C_{1,\infty} = C_\infty$ and $C_{2,\infty} = 2\ C_\infty$.

Eq. (53) indicates that if the electric potential, Ψ, is negative, the first term in the square bracket of the right hand side is much greater than the second term, i.e., the valence of positive ions dominates the potential distribution; otherwise the valence of negative ions controls the Debye length. Such an analysis agrees well with our numerical results that the valence and the concentration of the counter-ions dominate the Debye length. A greater valence of the counter-ions leads to a smaller Debye length. Therefore the definition in Eq. (52) is only valid for 1:1 electrolyte solutions.

5. Conclusions

In this contribution, we developed a coupled multiple LBM framework to solve the dynamic model for electrokinetic flows in microchannels. The governing equation for each transport is solved by an LBM and the whole transport process is simulated through an iteration procedure. We solve all the governing equations on the same set of lattices with consistent boundary condition treatments. The present algorithm and codes have been validated by comparisons with the results from the lattice PB method for homogeneously charged channels when the ionic advection is negligible.

Using the present method, the applicability of the PB model for electrokinetic flows in microchannels is studied. For homogeneously charged long channels, the PB model can provide good predictions for electric potential distributions until the electric double layers fully overlap which occurs when the thickness of the EDL equals to the channel width. The electroosmotic velocity prediction from the PB model is even good when the thickness of the EDL is 10 times of the channel width. For heterogeneously charged microchannels, a high zeta potential will make the PB prediction breakdown since the electric potential distribution is not fully developed. Because the streamlines are not parallel to the surfaces any more, an enhanced velocity field may cause the PB model to fail. However the ionic diffusion coefficients do not have noticeable effects on the steady flows for either homogeneously or heterogeneously charged channels. For the first time, the effects of ionic valence of solvent have been studied on the electric potential and flow velocity distributions in homogeneously charged microchannels. It is found that the valence and the concentration of the counter-ions dominate the Debye length, the electrical potential distribution and ions transport. The present results may improve the understanding of the electrokinetic transport characteristics in microchannels.

Acknowledgments

This work is supported by LANL's LDRD Project 20080727PRD2, through the J. R. Oppenheimer Fellowship awarded to M.W. The authors would like to thank Dr. Wang JK and Prof. Chen SY for helpful discussions.

References

[1] W.B.J. Zimmerman, Multiphysics modelling with finite element methods, World Scientific Publication, New Jersey, 2006.
[2] K.A. Sharp, B. Honig, Electrostatic interactions in macromolecules – Theory and applications, Annual Review of Biophysics and Biophysical Chemistry 19 (1990) 301–332.
[3] D.Q. Li, Encyclopedia of Microfluidics and Nanofluidics, Springer-Verlag, New York, 2008.
[4] D.J. DePaolo, F.M. Orr, Jr., Basic Research needs for Geosciences: Facilitating 21st Century Energy Systems, Office of Basic Energy Sciences, US Department of Energy, 2007.
[5] C.Y. Wang, Fundamental models for fuel cell engineering, Chemical Reviews 104 (2004) 4727–4765.
[6] D.Q. Li, Electrokinetics in microfluidics, Academic, Oxford, 2004.
[7] J.H. LinkMasliyah, Electrokinetic and colloid transport phenomena, Wiley-Interscience, Hoboken, 2006.
[8] W.D. Bancroft, Applied Colloid Chemistry General Theory, McGraw-Hill Book Company, New York, 1926.
[9] D.A. Doyle, J.M. Cabral, R.A. Pfuetzner, A.L. Kuo, J.M. Gulbis, S.L. Cohen, B.T. Chait, R. MacKinnon, The structure of the potassium channel: molecular basis of K^+ conduction and selectivity, Science 280 (1998) 69–77.
[10] R.D. Coalson, M.G. Kurnikova, Poisson–Nernst–Planck theory approach to the calculation of current through biological ion channels, IEEE Transactions on Nanobioscience 4 (2005) 81–93.
[11] P.K. Wong, T.H. Wang, J.H. Deval, C.M. Ho, Electrokinetics in micro devices for biotechnology applications, IEEE–ASME Transactions on Mechatronics 9 (2004) 366–376.
[12] H.A. Stone, A.D. Stroock, A. Ajdari, Engineering flows in small devices: Microfluidics toward a lab-on-a-chip, Annual Review of Fluid Mechanics 36 (2004) 381–411.
[13] T.M. Squires, S.R. Quake, Microfluidics: fluid physics at the nanoliter scale, Reviews of Modern Physics 77 (2005) 977–1026.
[14] D. Danilov, P.H.L. Notten, Mathematical modelling of ionic transport in the electrolyte of li-ion batteries, Electrochimica Acta 53 (2008) 5569–5578.
[15] J. Wu, V. Srinivasan, J. Xu, C.Y. Wang, Newton–Krylov-multigrid algorithms for battery simulation, Journal of the Electrochemical Society 149 (2002) A1342–A1348.
[16] M.Z. Bazant, T.M. Squires, Induced-charge electrokinetic phenomena: theory and microfluidic applications, Physical Review Letters 92 (2004). Article no. 066101.
[17] S.H. Yao, J.G. Santiago, Porous glass electro-osmotic pumps: theory, Journal of Colloid and Interface Science 268 (2003) 133–142.
[18] M. Wang, J.K. Wang, S.Y. Chen, N. Pan, Electrokinetic pumping effects of charged porous media in microchannels using the lattice Poisson–Boltzmann method, Journal of Colloid and Interface Science 304 (2006) 246–253.
[19] M.H. Oddy, J.G. Santiago, J.C. Mikkelsen, Electrokinetic instability micromixing, Analytical Chemistry 73 (2001) 5822–5832.

Author's personal copy

[20] E. Biddiss, D. Erickson, D.Q. Li, Heterogeneous surface charge enhanced micromixing for electrokinetic flows, Analytical Chemistry 76 (2004) 3208–3213.
[21] J.K. Wang, M.R. Wang, Z.X. Li, Lattice Boltzmann simulations of mixing enhancement by the electro-osmotic flow in microchannels, Modern Physics Letters B 19 (2005) 1515–1518.
[22] G. Karniadakis, A. Beskok, N. Aluru, Microflows and nanoflows fundamentals and simulation, Springer, New York, 2005.
[23] M. Holst, N. Baker, F. Wang, Adaptive multilevel finite element solution of the Poisson–Boltzmann equation I. Algorithms and examples, Journal of Computational Chemistry 21 (2000) 1319–1342.
[24] D.Q. Li, Electro-viscous effects on pressure-driven liquid flow in microchannels, Colloids and Surfaces A – Physicochemical and Engineering Aspects 195 (2001) 35–57.
[25] Z.L. Guo, T.S. Zhao, Y. Shi, A lattice Boltzmann algorithm for electro-osmotic flows in microfluidic devices, Journal of Chemical Physics 122 (2005).
[26] J.K. Wang, M. Wang, Z.X. Li, Lattice Poisson–Boltzmann simulations of electro-osmotic flows in microchannels, Journal of Colloid and Interface Science 296 (2006) 729–736.
[27] L. Chen, M.J. Holst, J.C. Xu, The finite element approximation of the nonlinear Poisson–Boltzmann equation, SIAM Journal on Numerical Analysis 45 (2007) 2298–2320.
[28] Y. Shi, T.S. Zhao, Z.L. Guo, Lattice Boltzmann simulation of thermal electro-osmotic flows in micro/nanochannels, Journal of Computational and Theoretical Nanoscience 5 (2008) 236–246.
[29] V.G. Levich, Physico-Chemical Hydrodynamics, Prentice-Hall, New York, 1962.
[30] L.M. Fu, J.Y. Lin, R.J. Yang, Analysis of electro-osmotic flow with step change in zeta potential, Journal of Colloid and Interface Science 258 (2003) 266–275.
[31] W.L. Qu, D.Q. Li, A model for overlapped EDL fields, Journal of Colloid and Interface Science 224 (2000) 397–407.
[32] R.J. Yang, L.M. Fu, C.C. Hwang, Electro-osmotic entry flow in a microchannel, Journal of Colloid and Interface Science 244 (2001) 173–179.
[33] S. Kang, Y.K. Suh, Unsteady electro-osmotic channel flows with the nonoverlapped and overlapped electric double layers, Journal of Mechanical Science and Technology 20 (2006) 2250–2264.
[34] F. Baldessari, Electrokinetics in nanochannels – Part I. Electric double layer overlap channel-to-well equilibrium, Journal of Colloid and Interface Science 325 (2008) 526–538.
[35] E.Y.K. Ng, S.T. Tan, Study of EDL effect on 3-D developing flow in microchannel with Poisson–Boltzmann and Nernst–Planck models, International Journal for Numerical Methods in Engineering 71 (2007) 818–836.
[36] H.M. Park, J.S. Lee, T.W. Kim, Comparison of the Nernst–Planck model and the Poisson–Boltzmann model for electro-osmotic flows in microchannels, Journal of Colloid and Interface Science 315 (2007) 731–739.
[37] Z. Chen, Comparison of the mobile charge distribution models in mixed ionic–electronic conductors, Journal of the Electrochemical Society 151 (2004) A1576–A1583.
[38] B.Z. Lu, Y.C. Zhou, G.A. Huber, S.D. Bond, M.J. Holst, J.A. McCammon, Electrodiffusion: a continuum modeling framework for biomolecular systems with realistic spatiotemporal resolution, Journal of Chemical Physics 127 (2007). Article no. 135102.
[39] D. Hlushkou, D. Kandhai, U. Tallarek, Coupled lattice Boltzmann and finite-difference simulation of electroosmosis in microfluidic channels, International Journal for Numerical Methods in Fluids 46 (2004) 507–532.
[40] M. Wang, N. Pan, J.K. Wang, S.Y. Chen, Lattice Poisson–Boltzmann simulations of electro-osmotic flows in charged anisotropic porous media, Communications in Computational Physics 2 (2007) 1055–1070.
[41] X. He, N. Li, Lattice Boltzmann simulation of electrochemical systems, Computer Physics Communications 129 (2000) 158–166.
[42] J. Horbach, D. Frenkel, Lattice Boltzmann method for the simulation of transport phenomena in charged colloids, Physical Review E 64 (2001). Article no. 061507.
[43] P. Dutta, A. Beskok, Analytical solution of combined electro-osmotic/pressure driven flows in two-dimensional straight channels: finite debye layer effects, Analytical Chemistry 73 (2001) 1979–1986.
[44] P. Dutta, A. Beskok, T.C. Warburton, Numerical simulation of mixed electro-osmotic/pressure driven microflows, Numerical Heat Transfer Part A – Applications 41 (2002) 131–148.
[45] M.R. Wang, J.K. Wang, S.Y. Chen, Roughness and cavitations effects on electro-osmotic flows in rough microchannels using the lattice Poisson–Boltzmann methods, Journal of Computational Physics 226 (2007) 836–851.
[46] P.C. Lichtner, Principles and practice of reactive transport modeling, Material Research Society of Symposium on Proceedings 353 (1995) 117–130.
[47] B. Honig, N. A, Classical electrostatics in biology and chemistry, Science 268 (1995) 1144–1149.
[48] M.J. Holst, F. Saied, Numerical-solution of the nonlinear Poisson–Boltzmann equation – developing more robust and efficient methods, Journal of Computational Chemistry 16 (1995) 337–364.
[49] J.K. Wang, M. Wang, Z.X. Li, Lattice evolution solution for the nonlinear Poisson–Boltzmann equation in confined domains, Communications in Nonlinear Science and Numerical Simulation 13 (2008) 575–583.
[50] M. Wang, S. Chen, Electroosmosis in homogeneously charged micro- and nanoscale random porous media, Journal of Colloid and Interface Science 314 (2007) 264–273.
[51] S. Chen, G.D. Doolen, Lattice Boltzmann method for fluid flows, Annual Review of Fluid Mechanics 30 (1998) 329–364.
[52] Y.H. Qian, D. Dhumieres, P. Lallemand, Lattice BGK models for Navier–Stokes equation, Europhysics Letters 17 (1992) 479–484.
[53] S. Succi, The Lattice Boltzmann equation for fluid dynamics and beyond, Numerical Mathematics and Scientific Computation, Oxford University Press, 2001.
[54] Q.J. Kang, D.X. Zhang, S.Y. Chen, Displacement of a three-dimensional immiscible droplet in a duct, Journal of Fluid Mechanics 545 (2005) 41–66.
[55] A.J. Wagner, S. Loew, S. May, Influence of monolayer–monolayer coupling on the phase behavior of a fluid lipid bilayer, Biophysical Journal 93 (2007) 4268–4277.
[56] Q.J. Kang, P.C. Lichtner, D.X. Zhang, Lattice Boltzmann pore-scale model for multi-component reactive transport in porous media, Journal of Geophysical Research-Solid Earth 111 (2006). Article no. B05203.
[57] Q.J. Kang, D.X. Zhang, S.Y. Chen, Unified lattice Boltzmann method for flow in multiscale porous media, Physical Review E 66 (2002). Article no. 056307.
[58] H.B. Li, X.Y. Lu, H.P. Fang, Z.F. Lin, Simulation of multi-particle suspensions in a quasi-two-dimensional symmetric stenotic artery with Lattice Boltzmann method, Progress in Computational Fluid Dynamics 5 (2005) 65–74.
[59] C. Migliorini, Y.H. Qian, H.D. Chen, E.B. Brown, R.K. Jain, L.L. Munn, Red blood cells augment leukocyte rolling in a virtual blood vessel, Biophysical Journal 83 (2002) 1834–1841.
[60] C.H. Sun, C. Migliorini, L.L. Munn, Red blood cells initiate leukocyte rolling in postcapillary expansions: a lattice Boltzmann analysis, Biophysical Journal 85 (2003) 208–222.
[61] K. Connington, Q. Kang, H.S. Viswanathan, A.I. Abdel-Fattah, S. Chen, Peristaltic particle transport using the lattice Boltzmann method, Physics of Fluids 21 (2009) 053301.
[62] X.Y. He, L.S. Luo, Theory of the lattice Boltzmann method: from the Boltzmann equation to the lattice Boltzmann equation, Physical Review E 56 (1997) 6811–6817.
[63] H.D. Chen, S.Y. Chen, W.H. Matthaeus, Recovery of the Navier–Stokes equations using a lattice-gas Boltzmann method, Physical Review A 45 (1992) R5339–R5342.
[64] X. He, S. Chen, G.D. Doolen, A novel thermal model for the lattice Boltzmann method in incompressible limit, Journal of Computational Physics 146 (1998) 282–300.
[65] Y. Peng, C. Shu, Y.T. Chew, Simplified thermal lattice Boltzmann model for incompressible thermal flows, Physical Review E 68 (2003).

Author's personal copy

[66] J.K. Wang, M. Wang, Z.X. Li, A lattice Boltzmann algorithm for fluid–solid conjugate heat transfer, International Journal of Thermal Sciences 46 (2007) 228–234.
[67] T. Inamuro, M. Yoshino, F. Ogino, A non-slip boundary condition for lattice Boltzmann simulations, Physics of Fluids 7 (1995) 2928–2930.
[68] T. Inamuro, M. Yoshino, F. Ogino, A non-slip boundary condition for lattice Boltzmann simulations, Physics of Fluids 8 (1996) 1124 (vol. 7 (1995) 2928).
[69] A. D'Orazio, S. Succi, Boundary conditions for thermal lattice Boltzmann simulations, Computational Science – ICCS 2003, Pt I, Proceedings, 2003, pp. 977–986.
[70] A. D'Orazio, S. Succi, Simulating two-dimensional thermal channel flows by means of a lattice Boltzmann method with new boundary conditions, Future Generation Computer Systems 20 (2004) 935–944.
[71] R.B. Fair, Digital microfluidics: is a true lab-on-a-chip possible?, Microfluidics and Nanofluidics 3 (2007) 245–281
[72] V. Srinivasan, V.K. Pamula, R.B. Fair, An integrated digital microfluidic lab-on-a-chip for clinical diagnostics on human physiological fluids, Lab-on-a-Chip 4 (2004) 310–315.
[73] O. Zohar, I. Leizerson, U. Sivan, Short range attraction between two similarly charged silica surfaces, Physical Review Letters 96 (2006) 177802.
[74] S. Basuray, H.C. Chang, Induced dipoles and dielectrophoresis of nanocolloids in electrolytes, Physical Review E 75 (2007) 060501.
[75] S. Pennathur, J.G. Santiago, Electrokinetic transport in nanochannels 1. Theory, Analytical Chemistry 77 (2005) 6772–6781.